An Evaluation of the Spectral Characteristics of Switching Converters With Chaotic Carrier-Frequency Modulation

K. K. Tse, *Member, IEEE*, Raymond Wai-Man Ng, Henry Shu-Hung Chung, *Member, IEEE*, and S. Y. Ron Hui, *Fellow, IEEE*

***Abstract*—This paper presents an evaluation of the spectral characteristics of switching converters with a chaotic carrier-frequency modulation scheme (CCFMS). By incorporating a Chua's circuit (CC) into the pulsewidth modulator for driving the switches, three modulation schemes, including the standard pulsewidth modulation scheme, periodic carrier-frequency modulation scheme, and CCFMS, can be realized with the CC in equilibrium, limit cycle, and chaos, respectively. The property of frequency spreading in CCFMS is studied by using statistical analysis method. The developed model is applied to formulate the power spectral densities of the input current and the output voltage of the three basic dc/dc converters under CCFMS. Theoretical predictions are verified with experimental measurements.**

***Index Terms*—Chaotic switching techniques, dc/dc conversion, power electronics, pulsewidth modulation, random switching techniques, switching circuits.**

I. Introduction

With the introduction of the international electromagnetic compatibility directives, there is an increasing awareness of the electromagnetic interference (EMI) problems of switching converters. In recent years, different frequency-modulated switching schemes (FMSS) have been applied to the pulsewidth-modulated (PWM) converters. By dithering the switching frequency around the nominal value, the discrete harmonic power that usually exists in classical PWM scheme can be spread over a wider frequency range, so that no harmonics of significant magnitude exist. This results in spreading the conducted EMI.

FMSS can basically be classified into two major types, namely, the periodic carrier-frequency modulation scheme (PCFMS) and the random carrier-frequency modulation scheme (RCFMS). The PCFMS can be realized by modulating a fixed-frequency sinusoidal signal into the ramp generator in the pulsewidth modulator. The switching period is then varied periodically. The resultant input power spectra contain discrete harmonics at the multiples of the modulating frequency and the sidebands—due to the cross modulation. In the RCFMS, a random modulating signal is used. The switching period is randomly dithered, resulting in a continuous input power spectrum. However, randomized switching introduces low-frequency noise at the output, which is undesirable for converters requiring tight regulation.

It has been shown in [1]–[3] that RCFMS can effectively reduce acoustic noise in ac motor drive systems. For the switching power converters, EMI reduction can also be achieved with both PCFMS [4] and RCFMS [5]–[8]. PCFMS requires a sinusoidal modulating signal whilst RCFMS requires either a digital or analog noise generator. A digital-circuit-based pseudorandom signal generator, a microprocessor-based pseudorandom algorithm [9] or a reverse-biased transistor for generating thermal noise in wideband nature [8] can be used to provide the random variable in RCFMS.

This paper presents the use of the Chua's circuit (CC) to replace the frequency-modulation source [10], [11]. One of the capacitor voltages in the CC is chosen to modulate the switching frequency. By adjusting the component value in the CC, standard pulsewidth modulation scheme (SPWMS), pulse-code modulation scheme (PCMS), and chaotic carrier-frequency modulation scheme (CCFMS) can be realized with the CC in equilibrium, limit cycle, and chaos, respectively. The CCFMS is found to exhibit similar behaviors as the RCFMS in the high-frequency range, but CCFMS introduces lower level of low-frequency harmonics at the output than that of the RCFMS.

Section II revisits the operation of the CC. Section III shows the spectral characteristics of the generated chaotic signal and describes how the CC is used in the frequency modulation. Based on the statistical analysis technique for the RCFMS, Section IV derives a model to study the frequency-spreading property of the CCFMS. The developed model is applied to formulate and evaluate the power spectral densities (PSD) of the input current and the output voltage of three basic dc/dc converters with CCFMS in Section V. Theoretical predictions are verified with experimental measurements in Section VI.

II. Revisit of the CC

Fig. 1 shows the schematic of the CC in which the value of the voltage-controlled nonlinear resistor N_R significantly af-

Manuscript received June 4, 2001; revised May 7, 2002. Abstract published on the Internet November 20, 2002. This work was supported by the Research Grant Council of Hong Kong under CERG Project 9040266. The work of K. K. Tse was supported by a Croucher Foundation Fellowship.

K. K. Tse is with Johnson Electric, Hong Kong.

R. W.-M. Ng is with the Department of Electronic Engineering, City University of Hong Kong, Kowloon, Hong Kong, and also with ASTEC Custom Power (HK) Ltd., Kong Kong.

H. S.-H. Chung and S. Y. R. Hui are with the Department of Electronic Engineering, City University of Hong Kong, Kowloon, Hong Kong (e-mail: eeshc@cityu.edu.hk).

Digital Object Identifier 10.1109/TIE.2002.807659

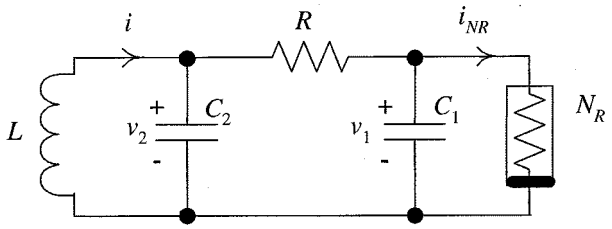

Fig. 1. Schematic of Chua's circuit.

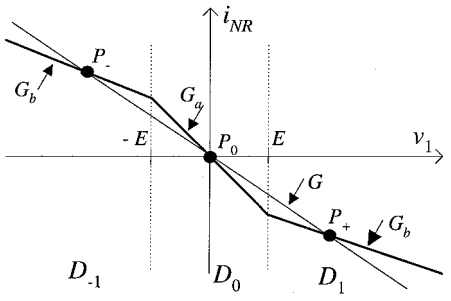

Fig. 2. Characteristic of nonlinear resistor N_R.

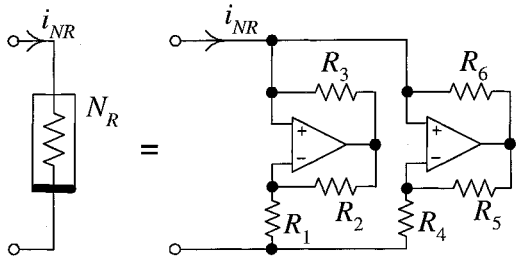

Fig. 3. Realization of nonlinear resistor using op-amps.

fects the circuit behavior. Characteristics of the nonlinear resistor current $i_{\rm NR}$ are shown in Fig. 2. Depending on the value of v_1, N_R acts as a negative piecewise-linear conductance in three segments. If the absolute value of v_1 is less than a threshold voltage E, N_R equals G_a. Otherwise, N_R equals G_b. Mathematically,

$$\begin{aligned}\frac{di}{dt} &= -\frac{1}{L}v_2\\ \frac{dv_2}{dt} &= \frac{1}{C_2}[i - G(v_2 - v_1)]\\ \frac{dv_1}{dt} &= \frac{1}{C_1}[G(v_2 - v_1) - i_{\rm NR}] \qquad \text{(1a)}\\ i_{\rm NR} &= f(v_1)\\ &= \begin{cases} G_b v_1 + (G_b - G_a)E, & \text{for } v_1 < -E\\ G_a v_1, & \text{for } -E \le v_1 \le E\\ G_b v_1 + (G_a - G_b)E, & \text{for } v_1 > E \end{cases} \qquad \text{(1b)}\end{aligned}$$

where $f(\cdot)$ is the function showing the relationships between $i_{\rm NR}$ and v_1, and $G = 1/R$.

The CC can be operated in three regions, namely, region "D_{-1}" for $v_1 < -E$, region "D_0" for $-E \le v_1 \le E$, and region "D_1" for $v_1 > E$. In each region, (1) can be described by three sets of state equations. The following dc load line for N_R can be formulated:

$$i_{\rm NR} = -Gv_1. \qquad (2)$$

As shown in Fig. 2, the intersection points between the load line in (2) and the characteristics of N_R determine the equilibrium points in each region. The equilibrium points are denoted by P_-, P_0, and P_+, respectively. It has been shown in [12] and [13] that

$$\begin{aligned}P_- &= \begin{bmatrix} \frac{G(G_b - G_a)E}{G+G_b} \\ 0 \\ \frac{(G_a - G_b)E}{G+G_b} \end{bmatrix}\\ P_0 &= \begin{bmatrix} 0 \\ 0 \\ 0 \end{bmatrix}\\ P_+ &= \begin{bmatrix} \frac{G(G_a - G_b)E}{G+G_b} \\ 0 \\ \frac{(G_b - G_a)E}{G+G_b} \end{bmatrix}. \qquad \text{(3a)}\end{aligned}$$

The eigenvalues in each operating region are determined by solving (1). The following characteristic equations can be obtained. For region "D_0,"

$$\lambda^3 + \left(\frac{G}{C_2} + \frac{G+G_a}{C_1}\right)\lambda^2 + \left(\frac{1}{LC_2} + \frac{GG_a}{C_1C_2}\right)\lambda + \frac{G+G_a}{LC_1C_2} = 0. \qquad \text{(3b)}$$

For regions "D_{-1}" and "D_1,"

$$\lambda^3 + \left(\frac{G}{C_2} + \frac{G+G_b}{C_1}\right)\lambda^2 + \left(\frac{1}{LC_2} + \frac{GG_b}{C_1C_2}\right)\lambda + \frac{G+G_a}{LC_1C_2} = 0. \qquad \text{(3c)}$$

The eigenvalues vary with R. Decreasing the value of R causes the CC to change from equilibrium to chaos. The practical circuit of N_R is shown in Fig. 3 [14], having dual operational amplifiers and six resistors (i.e., $R_1 \sim R_6$). G_a, G_b, and E are defined as follows:

$$\begin{aligned}G_a &= -\frac{R_2}{R_1R_3} - \frac{R_5}{R_4R_6}\\ G_b &= \frac{1}{R_3} - \frac{R_5}{R_4R_6}\\ E &= E_{\rm sat}\frac{R_1}{R_1 + R_2} \qquad (4)\end{aligned}$$

where $E_{\rm sat}$ is the saturation level of the operational amplifiers. Typically, the saturation level is about 8.3 V for the integrated circuit AD712 or TL082 with supply voltage at ± 9 V.

The component values of the CC are $L = 5.2$ mH, $C_1 = 22$ nF, $C_2 = 200$ nF, $G_a = -2$ mS, $E = 1$ V, and $G_b = -1.37$ mS. G can be adjusted from 1.47 to 1.6 mS (i.e., R is varied from 680 to 620 Ω). TL082 is used to model N_R. By solving (4), N_R can be modeled by using $R_1 = 3.3$ kΩ, $R_2 = 24$ kΩ, $R_3 = 12$ kΩ, $R_4 = 2.2$ kΩ, $R_5 = 240$ Ω, and $R_6 = 75$ Ω.

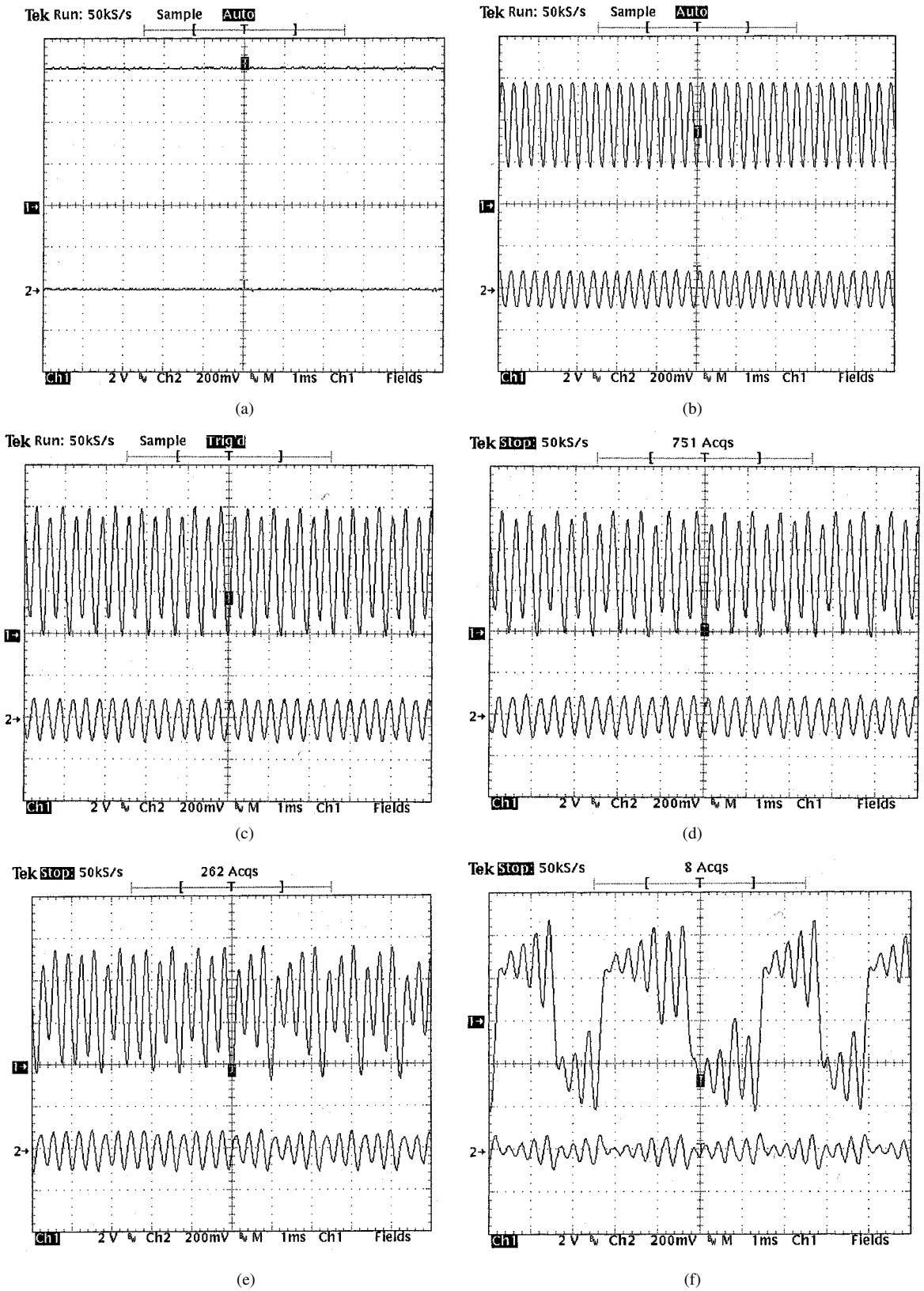

Fig. 4. Waveforms of Chua's circuit under various dynamical behaviors. Ch1: v_1 (2 V/div). Ch2: v_2 (2 V/div). Time: 1 ms/div. (a) Equilibrium at $R = 680\,\Omega$. (b) Period-1 limit cycle at $R = 645\,\Omega$. (c) Period-2 limit cycle at $R = 638\,\Omega$. (d) Period-4 limit cycle at $R = 637.5\,\Omega$. (e) Spiral chaos at $R = 635\,\Omega$. (f) double-scroll chaos at $R = 620$.

With different values of R, the measured waveforms of the capacitor voltages v_1 and v_2 are shown in Fig. 4. The equilibrium points and eigenvalues at each operating region are tabulated in Table I. When $R = 680\ \Omega$ [Fig. 4(a)], v_1 and v_2 stay at the equilibrium points P_+ or P_-, depending on the initial conditions. Both regions "D_1" and "D_{-1}" contain negative

TABLE I
EQUILIBRIUM POINTS AND EIGENVALUES FOR THREE OPERATING REGIONS

R (Ω)	Region	Equilibrium points at P_+, P_0, and P_-. [i $v2$ $v1$]$^{-1}$	Eigenvalues ($\times 10^3$)	Observation in circuit
680	D_1	[-10.23 × 10^3 0 6.93]$^{-1}$	-9.1; -1.39 ± j21.81	Equilibrium at either P_+ or P_-
	D_0	[0 0 0]$^{-1}$	33.88; -7.21 ± j26.63	
	D_{-1}	[10.23 × 10^3 0 -6.93]$^{-1}$	-9.1; -1.39 ± j21.81	
645	D_1	[-5.98 × 10^3 0 3.86]$^{-1}$	-16.2; 0.15 ± j21.98	Period-1 limit cycle with 3.5kHz
	D_0	[0 0 0]$^{-1}$	31.02; -7.79 ± j25.65	
	D_{-1}	[5.98 × 10^3 0 -3.86]$^{-1}$	-16.2; 0.15 ± j21.98	
638	D_1	[-5.53 × 10^3 0 3.53]$^{-1}$	-17.58; 0.41 ± j25.42	Period-2 limit cycle
	D_0	[0 0 0]$^{-1}$	30.41; -7.91 ± j25.42	
	D_{-1}	[5.53 × 10^3 0 -3.53]$^{-1}$	-17.58; 0.41 ± j25.42	
637.5	D_1	[-5.49 × 10^3 0 3.5]$^{-1}$	-17.68; 0.43 ± j22.1	Period-4 limit cycle
	D_0	[0 0 0]$^{-1}$	30.36; -7.92 ± j25.4	
	D_{-1}	[5.49 × 10^3 0 -3.5]$^{-1}$	-17.68; 0.43 ± j22.1	
635	D_1	[-5.35 × 10^3 0 3.4]$^{-1}$	-18.17; 0.52 ± j22.12	Spiral chaos
	D_0	[0 0 0]$^{-1}$	30.14; -7.97 ± j25.31	
	D_{-1}	[5.35 × 10^3 0 -3.4]$^{-1}$	-18.17; 0.52 ± j22.12	
620	D_1	[-4.62 × 10^3 0 2.86]$^{-1}$	-21.07; 1 ± j22.37	Double scroll chaos
	D_0	[0 0 0]$^{-1}$	28.77; -8.24 ± j24.75	
	D_{-1}	[4.62 × 10^3 0 -2.86]$^{-1}$	-21.07; 1 ± j22.37	

eigenvalues. When R is changed to 645 Ω [Fig. 4(b)], the real part of the complex conjugates of the eigenvalues becomes positive. Period-1 limit cycle (also called Hopf bifurcation) occurs. Also, depending on the initial conditions, the states can oscillate around the equilibrium points at P_+ or P_-, and exhibit a sinusoidal-like waveform at fixed frequency of 3.5 kHz, which can be calculated from the imaginary part of the complex conjugates of the eigenvalues in region "D_1" or "D_{-1}." When R is 638 Ω and 637.5 Ω [Fig. 4(c) and (d)], period-2 and period-4 limit cycles are observed, respectively. Further reducing R leads to spiral chaos [Fig. 4(e)] and double-scroll chaos [Fig. 4(f)]. At $R = 635\ \Omega$ [Fig. 4(e)], the circuit states fluctuate around the equilibrium points but no fixed limit cycle occurs. The state trajectories form a spiral attractor. At $R = 620\ \Omega$ [Fig. 4(f)], the states fluctuate around P_+ and P_- from time to time.

III. PSD OF THE CC OUTPUT AND PRACTICAL IMPLEMENTATION IN FMSS

Fig. 5 shows the three basic dc/dc converters, namely, the buck, boost, and buck–boost converters. The common method of controlling the output voltage V_{out} is to adjust the duty cycle and/or the switching frequency (or the switching period) of the main switch S. Practically, a PWM modulator [15], which consists of a sawtooth generator of constant frequency together with a comparator, can be used to determine the switching action of S.

Incorporation of chaotic behavior into the PWM scheme is depicted in Fig. 6. v_2 in Fig. 1 can be used to dither the switching frequency of a converter. It is sampled and is superimposed on a dc value, which determines the nominal switching frequency of the converter. The composite signal is connected to a voltage-controlled sawtooth generator. Thus, the switching period of the generated sawtooth waveform varies in accordance with the magnitude of the composite signal. The output of the error amplifier is compared to the generated sawtooth signal, and thus generating a PWM signal for the main switch in the

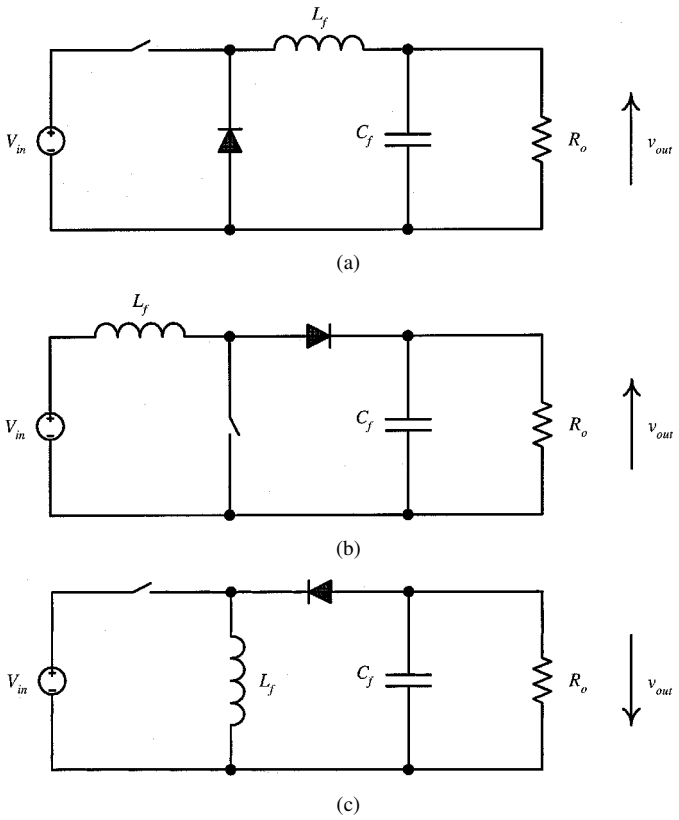

Fig. 5. Three basic types of dc/dc converters. (a) Buck converter. (b) Boost converter. (c) Buck–boost converter.

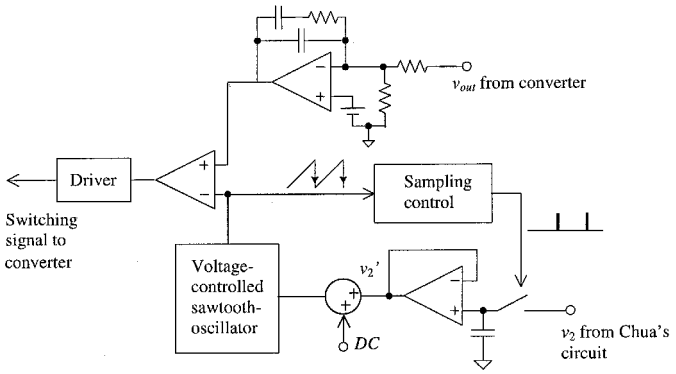

Fig. 6. Incorporation of chaotic behavior into the PWM scheme.

converter. It is important to note that the duty cycle remains unchanged even if the switching frequency is varying. Based on the fundamental considerations of sampled-data systems, a sampling rate of ten or more times the closed-loop bandwidth of the system is chosen for recovering the control signal. In analogy, the switching frequency of the power stage is selected to be higher than the oscillation frequency of the CC output in this application. In performing the experiment, the switching frequency was chosen to be 45 kHz while the oscillation frequency of the CC was 3.6 kHz. The ratio is 12.5.

Fig. 7(a) and (b) shows the experimental amplitude distributions of the sampled v_2 (i.e., v_2') in Fig. 6 when the CC is in period-1 limit cycle and chaos, respectively. The figures are extracted from a Tektronix TDS 784C oscilloscope. The shaded area on the left-hand side, which is displayed together with the

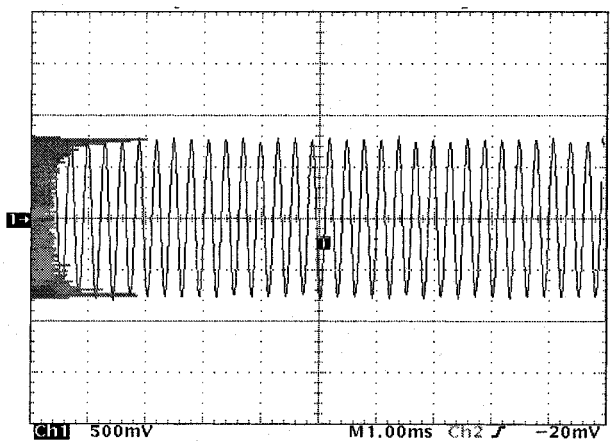

(a)

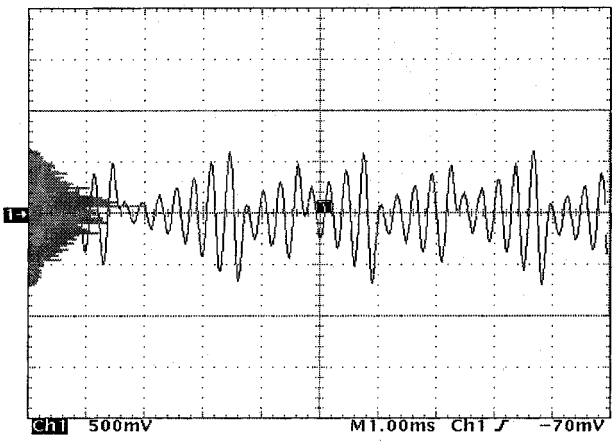

(b)

Fig. 7. Amplitude distribution under different operating modes. (a) Period-1 limit cycle. (b) Chaotic operation.

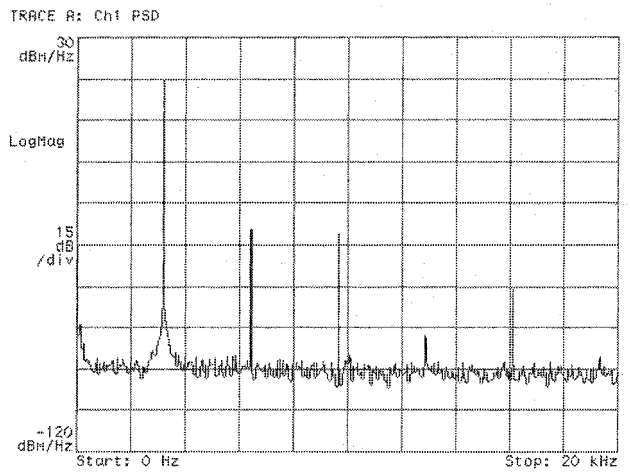

(a)

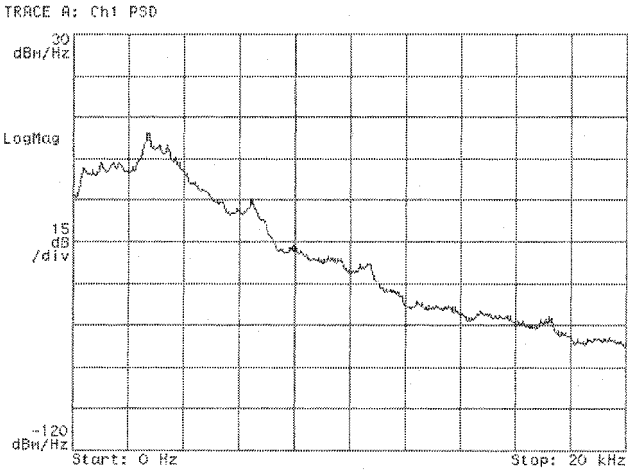

(b)

Fig. 8. PSD of v_2 under different operating modes. (a) Period-1 limit cycle. (b) Chaotic operation.

time waveform, is the histogram of the vertical values of v_2'. The horizontal span at a vertical position represents the number of occurrence of that particular value of v_2'. The value of v_2' is concentrated on the positive and negative peak values [16] in the period-1 limit cycle and it has a nearly triangular distribution in chaotic operation.

Fig. 8(a) and (b) shows the power spectral densities (PSDs) of the waveforms in Fig. 7. The PSD contains discrete harmonics in period-1 limit cycle [Fig. 8(a)] and becomes continuous spectra in chaotic operation [Fig. 8(b)]. In other words, the PWM signal generated by the circuit shown in Fig. 6, can exhibit different spectral distributions under different operating modes. In particular, if the signal is chaotic, the harmonic power can be spread over the spectrum and the peak level of the PSD becomes less than that of the classical PWM scheme. Discrete harmonics can, therefore, be significantly reduced. The harmonic power is spread continuously over the spectrum. The nonrepetitive nature of the signal in Fig. 7(b) and the continuous spectrum in Fig. 8(b) can be approximated by using the RCFMS with fixed duty cycle switching scheme.

IV. Mathematical Analysis Under CCFMS

Based on the analysis for RCFMS, a mathematical function shown in Fig. 9 is used to model the probability density function

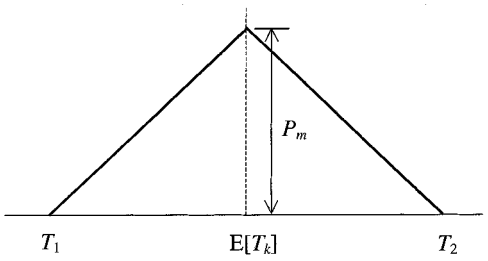

Fig. 9. Probability density function of the switching period.

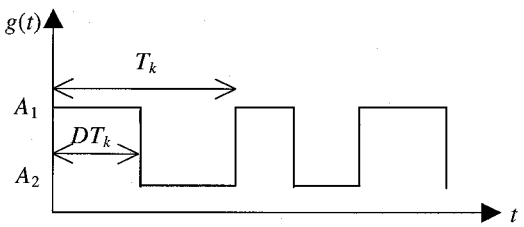

Fig. 10. Waveform of a PWM pulse train with chaotic switching.

of the period T_k of the kth switching cycle in Fig. 7(b). T_k varies between a minimum possible value T_1 and maximum possible value T_2. Fig. 10 shows the waveform of a PWM pulse train $g(t)$. $g(t)$ has two discrete levels, namely, A_1 and A_2.

For studying the effectiveness of the stochastic variable (i.e., the switching period T_k), an amplitude variation level $\Re$ is defined as

$$\Re = \frac{T_2 - T_1}{E[T_k]}. \tag{5}$$

Thus, the triangular probability density function in Fig. 9 is defined for a given $\Re$, since the area under the triangle is unity.

The PSD of the PWM pulse train in Fig. 10 can be shown to be equal to

$$S_p(f,\Re) = \frac{1}{E[T_k]} \times \left\{ E[|G(f)|^2] + 2\mathrm{Re}\left\{ \frac{E[G(f)e^{j2\pi f T_k}]E[G^*(f)]}{1 - E[e^{j2\pi f T_k}]} \right\} \right\} \tag{6}$$

where $G^*(f)$ is the complex conjugate of $G(f)$. $P(T_k)$ is probability density function of in Fig. 9. Detailed proof of (6) is shown in the Appendix. All expected terms in (6) can be expressed as follows:

$$\begin{aligned} G(f) =& A_1 \int_0^{DT_k} e^{-j2\pi f t} dt + A_2 \int_{DT_k}^{T_k} e^{-j2\pi f t} dt \\ =& \frac{j}{2\pi f} \left[(A_1 - A_2) e^{-j2\pi f D T_k} \right. \\ & \left. - A_1 + A_2 e^{-j2\pi f T_k} \right] \end{aligned} \tag{7}$$

$$P(T_k) = \begin{cases} P_m^2 (T_k - T_1); & T_1 \le T_k \le E[T_k] \\ -P_m^2 (T_k - T_2); & E[T_k] \le T_k \le T_2 \end{cases} \tag{8}$$

where $E[T_k] = (T_2 + T_1)/2$ and $P_m = 2/(T_2 + T_1)$. Thus,

$$E[|G(f)|^2] = \int_{T_1}^{T_2} P(T_k) G(f) G^*(f) dT_k \tag{9}$$

$$E[G(f)e^{j2\pi f T_k}] = \int_{T_1}^{T_2} P(T_k) G(f) e^{j2\pi f T_k} dT_k \tag{10}$$

$$E[G^*(f)] = \int_{T_1}^{T_2} P(T_k) G^*(f) dT_k \tag{11}$$

$$E[e^{j2\pi f T_k}] = \int_{T_1}^{T_2} P(T_k) e^{j2\pi f T_k} dT_k. \tag{12}$$

For the input current of the buck converter, A_1 equals [Output Power/$(D v_{\mathrm{in}})$] and A_2 equals zero (D is the nominal duty cycle). Equations (9)–(12) can be rewritten as follows:

$$\begin{aligned} &E[|G(f)|^2] \\ &= 2\left(\frac{A_1 P_m}{2\pi f}\right)^2 \\ &\quad \times \left\{ \left[\frac{T_k^2}{2} - T_1 T_k - \frac{T_k - T_1}{2\pi f} \sin(2\pi f D T_k) \right. \right. \\ &\qquad \left. \left. - \frac{1}{(2\pi f D)^2} \cos(2\pi f D T_k) \right] \right|_{T_1}^{E[T_k]} \\ &\qquad - \left[\frac{T_k^2}{2} - T_2 T_k - \frac{T_k - T_2}{2\pi f} \sin(2\pi f D T_k) \right. \\ &\qquad \left. \left. - \frac{1}{(2\pi f D)^2} \cos(2\pi f D T_k) \right] \right|_{E[T_k]}^{T_2} \Bigg\} \end{aligned} \tag{13}$$

and

$$\begin{aligned} &E[G(f)e^{j2\pi f T_k}] \\ &= \frac{j A_1 P_m^2}{2\pi f} \\ &\quad \times \left\{ \left[\left(\frac{T_k - T_1}{j2\pi f(1-D)} + \frac{1}{[2\pi f(1-D)]^2} \right) \right. \right. \\ &\qquad \times e^{j2\pi f(1-D)T_k} - \left(\frac{T_k - T_1}{j2\pi f} + \frac{1}{(2\pi f)^2} \right) \\ &\qquad \left. \left. \times e^{j2\pi f T_k} \right] \right|_{T_1}^{E[T_k]} \\ &\qquad - \left[\left(\frac{T_k - T_2}{j2\pi f(1-D)} + \frac{1}{[2\pi f(1-D)]^2} \right) \right. \\ &\qquad \times e^{j2\pi f(1-D)T_k} - \left(\frac{T_k - T_2}{j2\pi f} + \frac{1}{(2\pi f)^2} \right) \\ &\qquad \left. \left. \times e^{j2\pi f T_k} \right] \right|_{E[T_k]}^{T_2} \Bigg\} \end{aligned} \tag{14}$$

$$\begin{aligned} &E[G^*(f)] \\ &= -\frac{j A_1 P_m^2}{2\pi f} \\ &\quad \times \left\{ \left[\left(\frac{T_k - T_1}{j2\pi f D} + \frac{1}{(2\pi f D)^2} \right) \right. \right. \\ &\qquad \left. \left. \times e^{j2\pi f D T_k} - \frac{T_k^2}{2} + T_1 T_k \right] \right|_{T_1}^{E[T_k]} \\ &\qquad - \left[\left(\frac{T_k - T_2}{j2\pi f D} + \frac{1}{(2\pi f D)^2} \right) \right. \\ &\qquad \left. \left. \times e^{j2\pi f D T_k} - \frac{T_k^2}{2} + T_2 T_k \right] \right|_{E[T_k]}^{T_2} \Bigg\} \end{aligned} \tag{15}$$

$$\begin{aligned} &E[e^{j2\pi f T_k}] \\ &= P_m^2 \\ &\quad \times \left\{ \left(\frac{T_k - T_1}{j2\pi f} + \frac{1}{(2\pi f)^2} \right) e^{j2\pi f T_k} \right|_{T_1}^{E[T_k]} \\ &\qquad \left. - \left(\frac{T_k - T_2}{j2\pi f} + \frac{1}{(2\pi f)^2} \right) e^{j2\pi f T_k} \right|_{E[T_k]}^{T_2} \Bigg\}. \end{aligned} \tag{16}$$

As depicted in Fig. 11(a), a dc/dc converter can be considered as a low-pass filter fed by different types of input sources, which are dependent on the circuit configuration. With the aid of Table II, the transformed circuits are shown in Fig. 11.

Denote $H(f)$ as the transfer function of the filter. The PSD of the noise output $S_{n_o}(f,\Re)$ of the converter can be shown to be [17]

$$S_{n_o}(f,\Re) = S_p(f,\Re)|H(f)|^2, \qquad f \neq 0. \tag{17}$$

Noise power is calculated by integrating $S_{n_o}(f,\Re)$ over the spectrum. Hence, the root-mean-square value of the noise ripple $v(N)$ in the converter output is

$$v_N(\Re) = \left[\int_{-\infty}^{\infty} S_p(f,\Re)|H(f)|^2 df \right]^{1/2}, \qquad f \neq 0. \tag{18}$$

TABLE II
TRANSFER CHARACTERISTICS OF VARIOUS DC/DC CONVERTERS

Converters	Source of g	$H(f)$
Buck	Diode voltage	$\frac{v_{out}}{v_D}(f)=\frac{1+2\pi f\, r_C C_f}{L_f C_f\left[j2\pi f(\frac{1}{RC_f}+\frac{r_L+r_C}{L_f})-(2\pi f)^2+\frac{1}{L_f C_f}(1+\frac{r_L}{R})\right]}$
Boost	Diode current	$\frac{v_{out}}{i_D}(f)=\frac{R(1+j2\pi f\, r_C C_f)}{1+j2\pi f(r_C+R)C_f}$
Buck-boost	Diode current	$\frac{v_{out}}{i_D}(f)=\frac{R(1+j2\pi f\, r_C C_f)}{1+j2\pi f(r_C+R)C_f}$

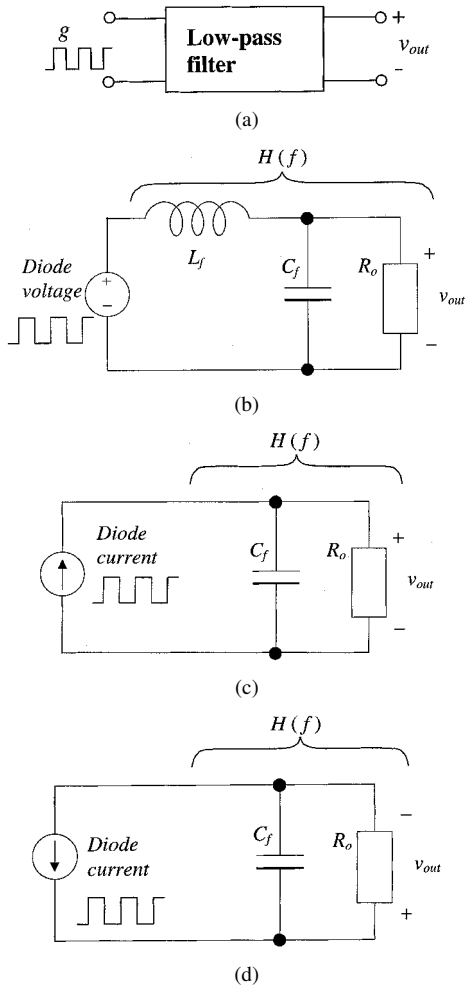

Fig. 11. Equivalent circuit of dc/dc converters. (a) Basic configuration. (b) Buck converter. (c) Boost converter. (d) Buck–boost converter.

Due to the rapid roll-off characteristics in $|H(f)|^2$ at high-frequency range, v_N can be approximated by

$$v_N(\Re)=\left[2\int_0^{2f_S} S_p(f,\Re)|H(f)|^2 df\right]^{1/2}, \qquad f\neq 0. \tag{19}$$

Only the continuous component and the dc component exist over the spectrum. Thus,

$$v_N=\left[\frac{4f_S}{N}\sum_{k=1}^{N} S_p^C\left(\frac{2kf_S}{N},\Re\right)\left|H\left(\frac{2kf_S}{N}\right)\right|^2\right]^{1/2} \tag{20}$$

where N is the number of frequency points over the range of $[0,2f_S]$.

V. EVALUATION OF THE PSD WITH CCFMS

The three basic converters in Fig. 5 are studied. The component values are $L_f=500\ \mu$H, $r_L=0.25\ \Omega$, $C_f=220\ \mu$F, $r_C=0.5\ \Omega$, and $R=5\ \Omega$. $v_{\rm in}$ is 22 V. The nominal switching frequency f_S is 45 kHz and duty cycle is 0.55. The PSDs of the input currents of the three converters are obtained by using PSIM 4.0 [18]. The simulated data are processed by Matlab [19], in order to calculate the corresponding PSDs. The results are shown in Fig. 12. Instead of containing discrete harmonics, the PSD's of the three converters' input currents are all in continuous spectra. Fig. 13 shows the theoretical prediction of the input current PSD of the buck converter using (6) with $\Re=0.35$. Figs. 12(a) and 13 are in close agreement at the high-frequency range. However, discrepancies occur in the low-frequency range, which will be explained in the following.

Fig. 14 shows the variations of the PSD of the diode voltage v_D of the buck converter with respect to the changes in $\Re$. $\Re$ is changed from 0 to 0.4. When $\Re$ is zero, the PSD is the same as the PSD of the SPWMS. As $\Re$ increases, the harmonic spectrum is gradually spread over. No significant improvements in spreading high-frequency harmonics are observed when $\Re$ is larger than 0.35. Fig. 15 shows the simulated low-frequency characteristic of v_D when $\Re$ is 0.35. The prediction will be verified with the experimental one in Section VI.

VI. EXPERIMENTAL VERIFICATIONS

A buck converter was tested and the PSDs were recorded by the HP 8941 spectrum analyzer with resolution bandwidth of 300 Hz. A current probe with sensitivity of 20 mV/A is used to measure the converter input current. Thus, the measured PSD

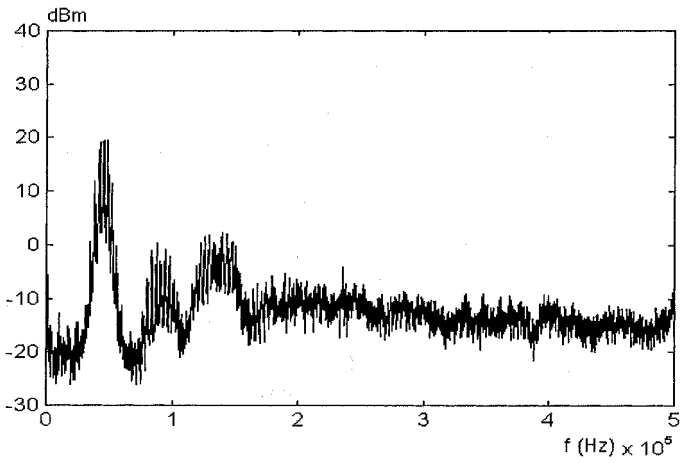

(a)

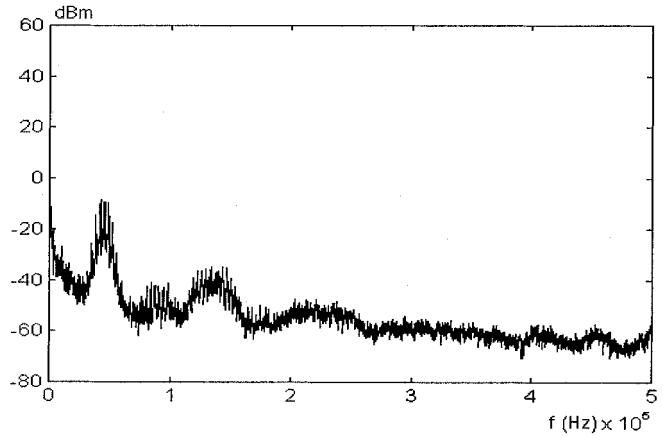

(b)

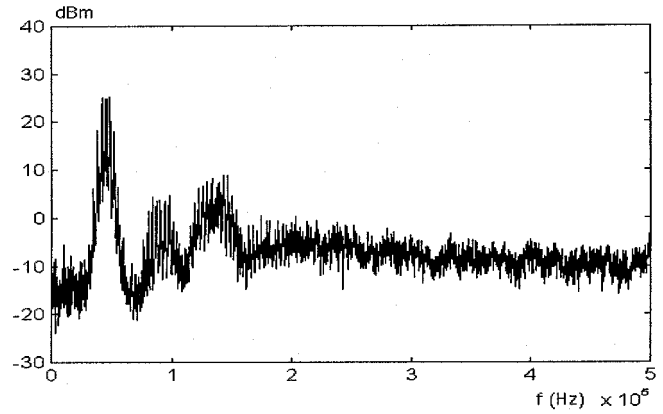

(c)

Fig. 12. PSD of input current of the three power converters under chaotic switching. (a) Buck converter. (b) Boost converter. (c) Buck–boost converter.

S_{meas} equals the sum of the actual PSD S and the conversion factor of the current probe. That is,

$$S_{\text{meas}} = S + 20\log 20 \times 10^{-3} = S - 34 \text{ dB}. \qquad (21)$$

Fig. 16 shows the measured PSD when the CC is in equilibrium, period-1 limit cycle, and chaos. Under chaotic operation, the PSD is in close agreement with the predictions in Figs. 12(a) and 13. Discrete harmonics are observed at equilibrium [Fig. 16(a)] and period-1 limit cycle [Fig. 16(b)]. When the switching frequency becomes chaotic [Fig. 16(c)], the power of the switching harmonics is well spread over.

Fig. 17 shows the low-frequency PSD of v_D under the CCFMS and the RCFMS. The modulating signal in the RCFMS is shown in Fig. 18. A 10:1 probe is used to pick up

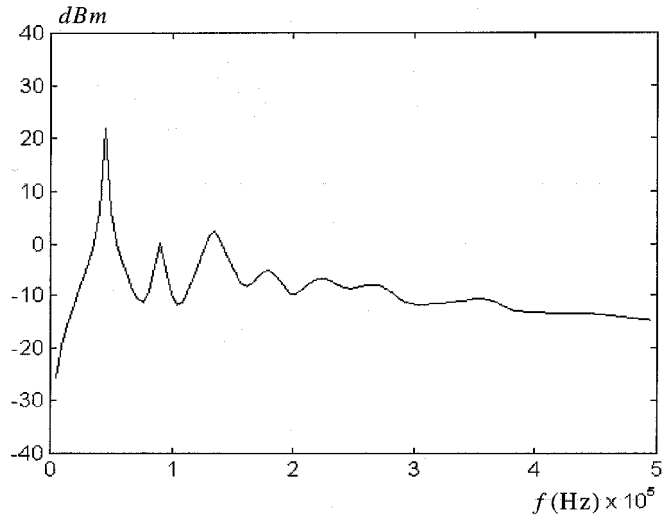

Fig. 13. Theoretical prediction of the input current PSD using (6) when $\Re = 0.35$.

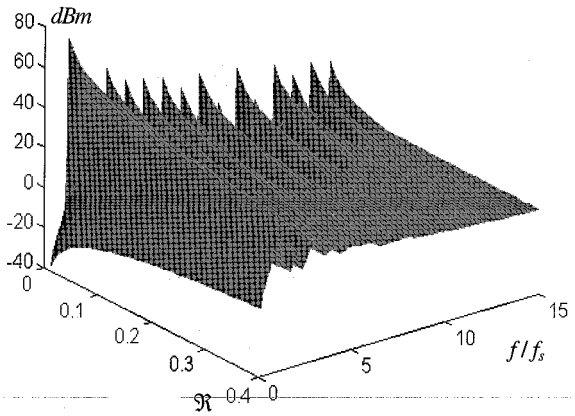

Fig. 14. PSD of the diode voltage with respect to the changes in $\Re$.

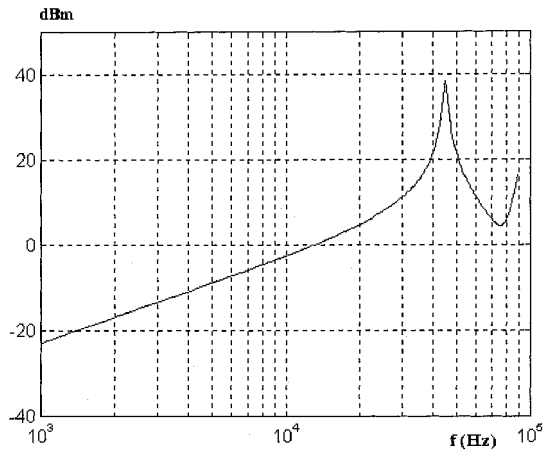

Fig. 15. Simulated low-frequency characteristic of the diode voltage with RCFMS and $\Re = 0.35$.

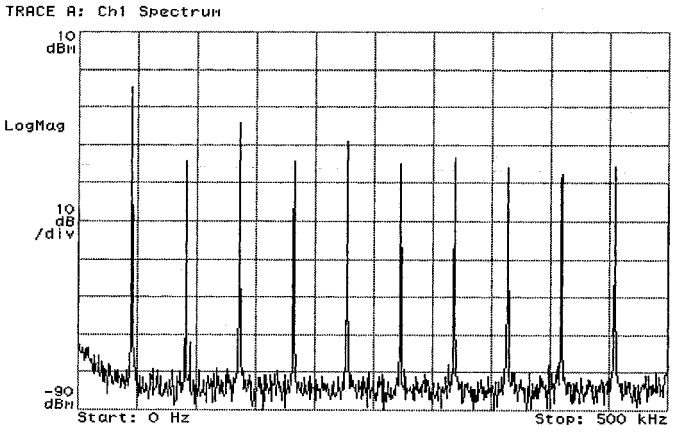

(a)

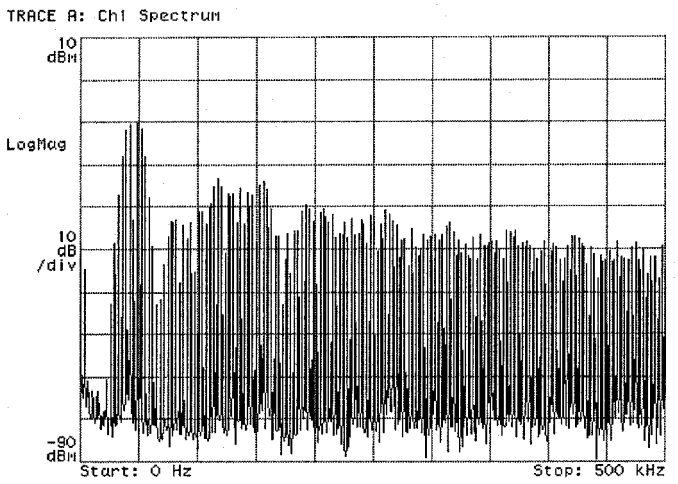

(b)

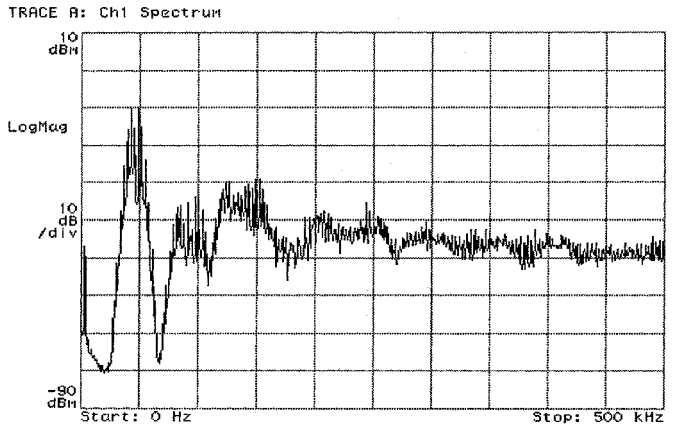

(c)

Fig. 16. Measured PSD of input current of buck converter. (a) Equilibrium. (b) Period-1 limit cycle. (c) Chaos.

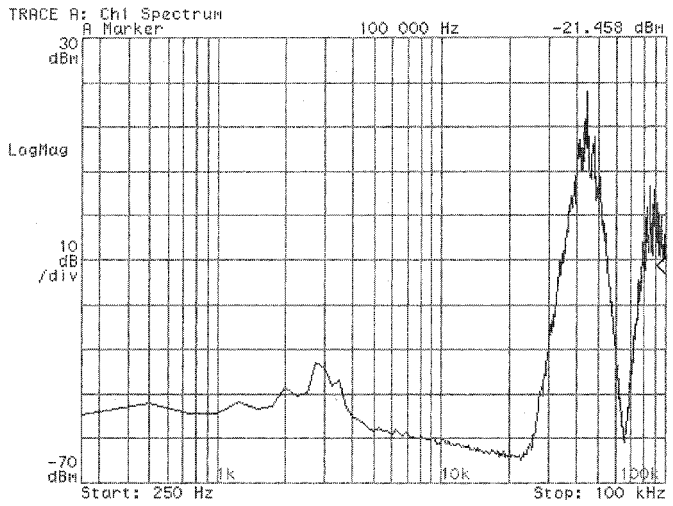

(a)

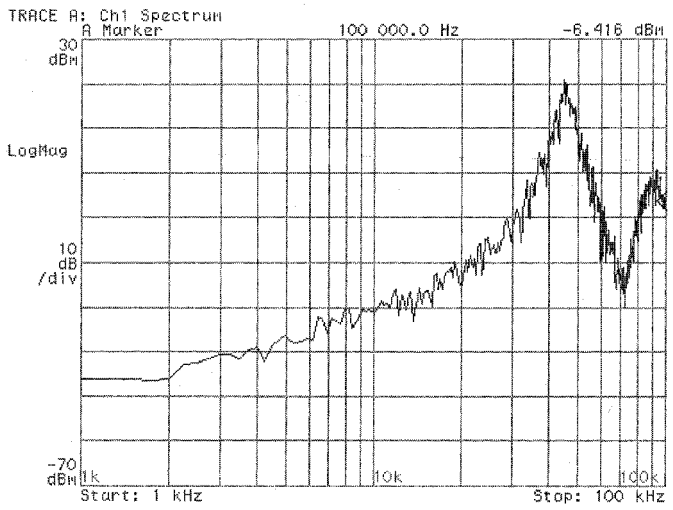

(b)

Fig. 17. Measured PSD of diode voltage in low-frequency range. (a) CCFMS. (b) RCFMS.

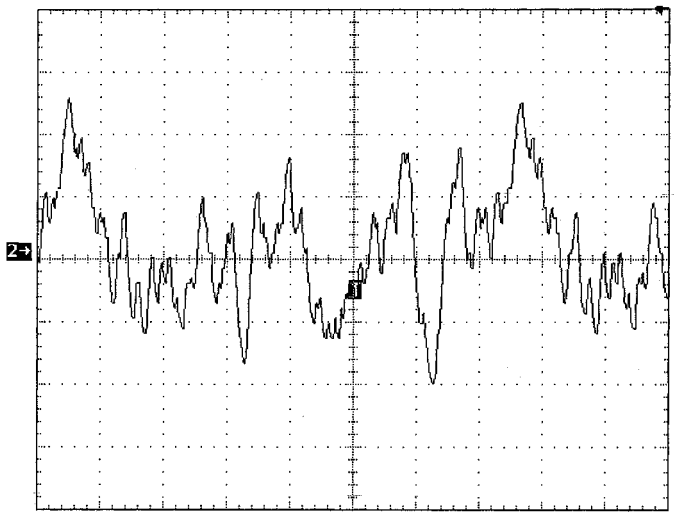

Fig. 18. Modulating signal in RCFMS (Ch2: 0.2 V/div; timebase: 1 ms/div).

the signal in the measurement. Thus, a 20 dB difference is introduced between the measurement PSD and the prediction. Comparing the PSDs with Fig. 15, the low-frequency spectral characteristic of the CCFMS is different from the prediction using RCFMS. The low-frequency spectral magnitude in the RCFMS is higher than that in the CCFMS. By comparing Fig. 7(b) with Fig. 18, the CC output signal oscillates alternatively and symmetrically around the origin (even if the amplitude varies). The probability of generating biased and/or low-frequency harmonic components with CCFMS is lower than that

of the RCFMS. Hence, even if the CCFMS and RCFMS are stochastic in nature and exhibit the same probability density function, their spectral behaviors are slightly different because the time-domain variation cannot be obtained from the probability density function. Nevertheless, CCFMS has the advantages that it does not introduce significant low-frequency harmonics and that it improves high-frequency characteristics in the SPWMS.

VII. Conclusions

A CCFMS has been analyzed and evaluated. The CC has been incorporated into the switching control of the power converters. The input current and output voltage power spectral densities under different operating regions have been studied theoretically and experimentally. By controlling the dynamics of the CC, it has been shown that CCFMS hybridizes the features of PCFMS and RCFMS. Experimental results have confirmed that CCFMS is an alternative way for reducing the amplitudes of switching harmonics. Most importantly, the CCFMS introduces less low-frequency harmonics at the output than the RCFMS. Apart from studying the effect of chaotic frequency modulation on switching converters, this paper also provides the methodology of analysis. Readers can use other kinds of chaotic generators with similar analysis method. Further research will be dedicated to studying the sensitivities of the PSD to the circuit parameters.

Appendix

A. Proof of (6)

Considering the generic switching cycle k in Fig. 10, the switching waveform $g_k(t-t_k)$, can be expressed as

$$g_k(t-t_k)=\begin{cases} A_1, & \text{for } t_k \le t < DT_k \\ A_2, & \text{for } DT_k \le t > T_k \\ 0, & \text{elsewhere} \end{cases} \tag{A.1}$$

where T_k is a randomized switching period. A general expression for $g(t)$ is

$$g(t)=\lim_{N\to\infty}\sum_{k=1}^{N} g_k(t-t_k). \tag{A.2}$$

The autocorrelation of $g(t)$ is defined as

$$R_g(\tau)=E\left[\lim_{T_o\to\infty}\frac{1}{T_o}\int_0^{T_o} g(t)g(t+\tau)dt\right] \tag{A.3}$$

where $E[\cdot]$ is the expected value of the quantity inside the bracket. T_o is the observation interval, containing N expected value of T_k. That is,

$$T_o = NE[T_k]. \tag{A.4}$$

By substituting (A.2) and (A.4) into (A.3),

$$R_g(\tau)=\lim_{N\to\infty}\frac{1}{NE[T_k]}\sum_{k=1}^{N}\sum_{l=1}^{N}E \times\left[\int_0^{\infty} g_k(t-t_k)g_l(t+\tau-t_l)dt\right]. \tag{A.5}$$

If $G_k(f)$ and $G_l(f)$ denote the Fourier transform of $g_k(t)$ and $g_l(t)$, respectively, and Γ denotes the time integral in (A.5),

$$\begin{aligned}\Gamma &= \int_0^{\infty} g_k(t-t_k)g_l(t+\tau-t_l)dt \\ &= \int_0^{\infty}\left[\int_{-\infty}^{\infty} G_k(f)e^{-j2\pi f t_k}e^{j2\pi f t}df\right] \\ &\quad\cdot\left[\int_{-\infty}^{\infty} G_l(f')e^{j2\pi f'(\tau-t_l)}e^{j2\pi f' t}df'\right]dt \\ &= \int_0^{\infty}\int_{-\infty}^{\infty}\int_{-\infty}^{\infty} e^{j2\pi(f+f)t}dt G_k(f)G_l(f') \\ &\quad\times e^{-j2\pi f t_k}e^{j2\pi f'(\tau-t_l)}df df'. \end{aligned} \tag{A.6}$$

Referring to [3],

$$\int_{-\infty}^{\infty} e^{j2\pi(f+f)t}dt = \delta(f'+f). \tag{A.7}$$

Equation (A.6) can be expressed as

$$\begin{aligned}\Gamma &= \int_0^{\infty}\int_{-\infty}^{\infty}\delta(f+f)G_k(f)G_l(f') \\ &\quad\times e^{-j2\pi f t_k}e^{j2\pi f'(\tau-t_l)}df df' \\ &= \int_0^{\infty} G_k(-f')G_l(f')e^{j2\pi f'\tau}e^{j2\pi f'(t_k-t_l)}df' \\ &= \int_0^{\infty} G_k^*(f)G_l(f)e^{j2\pi f\tau}e^{j2\pi f(t_k-t_l)}df. \end{aligned} \tag{A.8}$$

Hence, the autocorrelation of g can be expressed as

$$R_g(\tau)=\lim_{N\to\infty}\frac{1}{NE[T_k]}\sum_{k=1}^{N}\sum_{l=1}^{N}\int_0^{\infty} E \times\left[G_l(f)G_k^*(f)e^{j2\pi f(t_k-t_l)}\right]e^{j2\pi f\tau}df. \tag{A.9}$$

Based on the Wiener–Khinchin theorem [20], the PSD of a signal $S(f)$ is the Fourier transform of its autocorrelation function $R(\tau)$. Conversely, the autocorrelation can be given by the inverse Fourier transform of the PSD. That is,

$$S(f)=\int_{-\infty}^{\infty} R(\tau)e^{-j2\pi f\tau}d\tau \tag{A.10}$$

and

$$R(\tau)=\int_{-\infty}^{\infty} S(f)e^{j2\pi f\tau}df. \tag{A.11}$$

With this relationship, the PSD of g over the range of positive frequency $S_p(f,\Re_{\mathrm{RCFM}})$ is easily observed from (A.9), in terms of the randomness level of T_k, i.e.,

$$S_p(f,\Re_{\mathrm{RCFM}})=\lim_{N\to\infty}\frac{1}{NE[T_k]}\sum_{k=1}^{N}\sum_{l=1}^{N}E \times\left[G_l(f)G_k^*(f)e^{j2\pi f(t_k-t_l)}\right]. \tag{A.12}$$

Consider $S_\Sigma(f)$ denoting the double summation of the expected term in (A.12),

$$S_p(f,\Re_{\mathrm{RCFM}})=\lim_{N\to\infty}\frac{1}{NE[T_k]}S_\Sigma(f) \tag{A.13}$$

where

$$\begin{aligned} S_\Sigma(f) =& \sum_{k=1}^{N}\sum_{l=1}^{N} E[G_l(f)G_k^*(f)e^{j2\pi f(t_k-t_l)}] \\ =& NE[|G(f)|^2] \\ &+ \sum_{k=1}^{N}\sum_{\substack{l=1\\ l\neq k}}^{N} E\left[G_l(f)G_k^*(f)e^{j2\pi f(t_k-t_l)}\right]. \end{aligned} \tag{A.14}$$

$G_l(f)$ is dependent on $e^{j2\pi f(t_k-t_l)}$ if

$$|t_k - t_l| = T_l \tag{A.15}$$

and $G_k^*(f)$ is dependent on $e^{j2\pi f(t_k-t_l)}$ if

$$|t_k - t_l| = T_k. \tag{A.16}$$

Hence, (A.14) can be shown to be

$$\begin{aligned} S_\Sigma(f) =& NE[|G(f)|^2] + 2(N-1) \\ &\times \mathrm{Re}\{E[G(f)]E[G^*(f)e^{j2\pi fT_k}]\} + \Phi_\Sigma(f) \end{aligned} \tag{A.17}$$

where

$$\begin{aligned} \Phi_\Sigma(f) =& G_1^*(f)\sum_{l=3}^{N} G_l(f)e^{j2\pi f(t_1-t_l)} \\ &+ G_2^*(f)\sum_{\substack{l=1\\ l\neq 1,2,3}}^{N} G_l(f)e^{j2\pi f(t_2-t_l)} \\ &+ G_3^*(f)\sum_{\substack{l=1\\ l\neq 2,3,4}}^{N} G_l(f)e^{j2\pi f(t_3-t_l)} \\ &+ \cdots + G_N^*(f)\sum_{l=1}^{N-2} G_l(f) \\ &\times e^{j2\pi f(t_N-t_l)}. \end{aligned} \tag{A.18}$$

Consider

$$\phi = E[e^{j2\pi fT_k}] \tag{A.19}$$

and

$$E[e^{j2\pi f(t_k-t_l)}] = \begin{cases} [\phi]^{k-l}, & \text{for } k > l \\ [\phi^*]^{l-k}, & \text{for } l > k. \end{cases} \tag{A.20}$$

Thus, (A.18) becomes a real number as

$$\begin{aligned} \Phi_\Sigma(f) =& 2\,\mathrm{Re}\{E[G^*(f)]E[G(f)e^{j2\pi fT_k}] \\ &\times (\phi + \\ &\phi + \phi^2 + \\ &\phi + \phi^2 + \phi^3 + \\ &\cdots + \\ &\phi + \phi^2 + \phi^3 + \phi^4 + \cdots + \phi^{N-2})\}. \end{aligned} \tag{A.21}$$

Since $|\phi| < 1$, (A.21) is simplified as

$$\begin{aligned} \Phi_\Sigma(f) =& 2\mathrm{Re}\left\{E[G^*(f)]E[G(f)e^{j2\pi fT_k}]\right. \\ &\left.\times \frac{\phi}{1-\phi}\left[(N-1) - \frac{1-\phi^{N-1}}{1-\phi}\right]\right\}. \end{aligned} \tag{A.22}$$

By substituting (A.22) into (A.17),

$$\begin{aligned} S_\Sigma(f) =& NE[|G(f)|^2] + 2(N-1) \\ &\times \mathrm{Re}\left\{E[G^*(f)]E[G(f)e^{j2\pi fT_k}]\right. \\ &\left.\times\left(1 + \frac{\phi}{1-\phi}\right)\right\} \\ &+ 2\mathrm{Re}\left\{E[G^*(f)]E[G(f)e^{j2\pi fT_k}]\right. \\ &\left.\times\frac{\phi(1-\phi^{N-1})}{(1-\phi)^2}\right\}. \end{aligned} \tag{A.23}$$

Finally, (A.13) becomes

$$\begin{aligned} S_p(f, \Re_{\mathrm{RCFM}}) =& \frac{1}{E[T_k]}\left(E[|G(f)|^2]\right. \\ &\left.+2\mathrm{Re}\left[\frac{E[G(f)e^{j2\pi fT_k}]E[G^*(f)]}{1-E[e^{j2\pi fT_k}]}\right]\right). \end{aligned} \tag{A.24}$$

REFERENCES

[1] S. Legowski and M. Trzynadlowski, "Power-Mosfet, hypersonic inverter with high-quality output current," in *IEEE APEC'90*, 1990, pp. 3–7.

[2] T. G. Habeter and D. M. Divan, "Acoustic noise reduction in sinusoidal PWM drives using a randomly modulated carrier," *IEEE Trans. Power Electron.*, vol. 6, pp. 356–363, May 1991.

[3] R. L. Kirlin, S. Kwok, S. Legowski, and A. M. Trzynadlowski, "Power spectra of a PWM inverter with randomized pulse position," *IEEE Trans. Power Electron.*, vol. 9, pp. 463–472, Sept. 1994.

[4] F. Lin and D. Y. Chen, "Reduction of power supply EMI emission by switching frequency modulation," *IEEE Trans. Power Electron.*, vol. 9, pp. 132–137, Jan. 1994.

[5] D. A. Stone and B. Chambers, "Effect of spread-spectrum modulation of switched mode power converter PWM carrier frequencies on conducted EMI," *Electron. Lett.*, vol. 31, no. 10, pp. 769–770, 1995.

[6] K. K. Tse, H. Chung, S. Y. R. Hui, and H. C. So, "A comparative investiation on the use of random modulation schemes for dc/dc converters," *IEEE Trans. Ind. Electron.*, vol. 47, pp. 253–263, Apr. 2000.

[7] ——, "Spectral characteristics of randomly switched PWM dc/dc converters operating in discontinuous conduction mode," *IEEE Trans. Ind. Electron.*, vol. 47, pp. 759–769, Aug. 2000.

[8] ——, "Analysis and Spectral characteristics of a spread-spectrum technique for conducted EMI suppression," *IEEE Trans. Power Electron.*, vol. 15, pp. 399–410, Mar. 2000.

[9] S. Y. R. Hui, I. Oppermann, and S. Sathiakumar, "Microprocessor-based random PWM schemes for DC-AC power conversion," *IEEE Trans. Power Electron.*, vol. 12, pp. 253–260, Mar. 1997.

[10] F. Ueno, I. Oota, and I. Harada, "A low-noise control circuit using Chua's circuit for a switching regulator," in *Proc. Eur. Conf. Circuit Theory and Design*, 1995, pp. 1149–1152.

[11] J. H. B. Deane and D. C. Hamill, "Improvement of power supply EMC by Chaos," *Electron. Lett.*, vol. 32, no. 12, p. 1045, 1996.

[12] M. P. Kennedy, "Three steps to chaos—Part I," *IEEE Trans. Circuits Systs. I*, vol. 40, pp. 640–656, Oct. 1993.

[13] M. P. Kennedy, "Three steps to chaos—Part II," *IEEE Trans. Circuits Systs. I*, vol. 40, pp. 657–674, Oct. 1993.

[14] R. N. Madan, *Chua's Circuit: A Paradigm of Chaos*, Singapore: World Scientific, 1993.

[15] N. Mohan, T. M. Undeland, and W. P. Robbins, *Power Electronics—Converters, Applications, and Design*. New York: Wiley, 1995.

[16] J. J. O'Reilly, *Telecommunication Principles*. London, U.K.: Chapman & Hall, 1991.

[17] A. Papoulis, *Probability Random Variables, and Stochastic Processes*. New York: McGraw-Hill, 1991.

[18] *PSIM User Manual*, Powersim Technologies Inc., Surrey, BC, Canada, 1998.
[19] T. P. Kraus, L. Shure, and J. N. Little, *Signal Processing Toolbox for Use With Matlab*. Natick, MA: The MathWorks Inc., 1994.
[20] D. Middleton, *An Introduction to Statistical Communication Theory*. New York: McGraw-Hill, 1988.

K. K. Tse (M'00) received the B.Eng. (Hons.) degree in electrical engineering from The Hong Kong Polytechnic University, Hong Kong, and the Ph.D. degree from City University of Hong Kong, Hong Kong, in 1995 and 2000, respectively.

He served as a Lecturer at the Hong Kong Institute of Vocational Education (Tsing Yi) (formerly Technical College) in 1998. From 1999 to 2001, he was a Research Fellow in the Electronic Engineering Department, City University of Hong Kong. Since June 2001, he has been with Johnson Electric, Hong Kong, where he is currently a Technical Specialist in the R&D area. He has authored more than 20 published technical papers in the areas of his research interests, which include new numerical model methods and computer-aided simulation techniques, EMI reduction using random switching schemes for dc–dc converters, and new maximum power tracking techniques for PV cells.

Dr. Tse received the First Prize in 1998 in the IEEE Postgraduate Student Paper Contest, Hong Kong Section, and the Third Prize in the 1999 Region 10 IEEE Postgraduate Student Paper Contest. He was a recipient of The Croucher Foundation Fellowship in 2000. In December 2000, he received the Silver Award in the Young Inventor Competition, jointly organized by the Far Eastern Economic Review and Hewlett Packard Company.

Raymond Wai-Man Ng was born in Hong Kong. He received the B.Eng. (Hons.) degree in electronic engineering in 1988 from City University of Hong Kong, Hong Kong, where he is currently working toward the Master of Philosophy degree.

In 1998, he joined ASTEC Custom Power (HK) Ltd., Kong Kong, as a Design Engineer. Since 2000, he has been the Application Engineer on Ericsson Power Module Team. His research interests are EMI and dc/dc conversion.

Henry Shu-Hung Chung (S'92–M'95) received the B.Eng. (with first class honors) degree in electrical engineering and the Ph.D. degree from The Hong Kong Polytechnic University, Hong Kong, in 1991 and 1994, respectively.

Since 1995, he has been with City University of Hong Kong, Hong Kong, where he is currently an Associate Professor in the Department of Electronic Engineering. His research interests include time- and frequency-domain analysis of power electronic circuits, switched-capacitor-based converters, random-switching techniques, digital audio amplifiers, soft-switching converters, and electronic ballast design. He has authored four research book chapters and more than 130 technical papers, including 70 refereed journal papers in the current research area, and is the holder of two U.S. patents.

Dr. Chung is currently the IEEE Student Branch Counselor at City University of Hong Kong and was Track Chair of the Technical Committee on Power Electronics Circuits and Power Systems of the IEEE Circuits and Systems Society in 1997–1998. He is presently an Associate Editor of the IEEE TRANSACTIONS ON CIRCUITS AND SYSTEMS—I: FUNDAMENTAL THEORY AND APPLICATIONS and the Guest Editor of the Special Issue on Analysis, Design and Applications of Switching Circuits and Systems. He was the recipient of the China Light and Power Prize and was awarded the Scholarship and Fellowship of the Sir Edward Youde Memorial Fund in 1991 and 1993, respectively. He was awarded the Grand Applied Research Excellence Award in 2001 from City University of Hong Kong.

S. Y. Ron Hui (SM'94–F'03) was born in Hong Kong in 1961. He received the B.Sc. (Hons.) degree in 1984 from the University of Birmingham, Birmingham, U.K., and the D.I.C. and Ph.D. degree in 1987 from Imperial College of Science and Technology, University of London, London, U.K.

He was a Lecturer in power electronics at the University of Nottingham, Nottingham, U.K., in 1987–1990. In 1990, he took up a lectureship at the University of Technology, Sydney, Australia, where he became a Senior Lecturer in 1991. He joined the University of Sydney in 1993 and was promoted to Reader of Electrical Engineering and Director of the Power Electronics and Drives Research Group in 1996. He is currently a Chair Professor of Electronic Engineering and an Associate Dean of the Faculty of Science and Engineering at City University of Hong Kong, Hong Kong. He has authored more than 150 published technical papers, including more than 80 refereed journal publications. His research interests include all aspects of power electronics.

Prof. Hui received the Teaching Excellence Award in 1999 and the Grand Applied Research Excellence Award in 2001 from City University of Hong Kong. He has been appointed an Honorary Professor by the University of Sydney since 2000.